Proceedings of 23rd IAEA FEC 2010, Daejon, Korea,
paper THW/P7-09, 11-16 October (2010)

Comparison of Quasi-linear and Exact Ion Cyclotron Resonant Heating Diffusion, With and Without Finite Width Ion Orbits

R.W. Harvey[1], Yu. V. Petrov[1], D.L. Green[2], E.F. Jaeger[3], P.T. Bonoli[4], D.B. Batchelor[2], L.A. Berry[2], J.C. Wright[4], A. Bader[4], and RF-SciDAC Group
[1]CompX, Del Mar, CA 92014, USA; [2]Oak Ridge National Laboratory, Oak Ridge, TN 37831, USA; *[3]Xcel Engineering, Oak Ridge, TN 37830, USA; [4]PSFC-MIT,Cambridge, MA 02139*
e-mail contact of main author: rwharvey@compxco.com

Abstract. This work investigates the validity of quasi-linear (QL) diffusion theory and the significance of finite ion orbit effects on Ion Cyclotron Resonant Heating (ICRH) in Tokamak plasmas. By comparing QL diffusion coefficients with exact values calculated by direct Lorentz orbit integration in full-wave RF electric fields (with the DC code), we examine the issues of (i) neglecting correlations between successive resonant surface crossings, and (ii) including a realistic toroidal antenna spectrum. The impact of finite ion orbits are assessed by examining moments of the ion distribution under a self-consistent full-wave / Monte-Carlo iterative calculation.

1. Introduction

The DC diffusion coefficient calculator numerically integrates the trajectories of ions launched from tokamak midplane points, equispaced in initial gyro-phase about given gyro-center and also in toroidal length along a given RF mode wavelength, and averages the resulting square of the velocity changes after one (or more) poloidal circuits in combined tokamak equilibrium and RF full wave fields from the AORSA full-wave code[1], to obtain the ICRF bounce-averaged diffusion tensor. This is carried out for a 3D array ($u_{\|}$, $u_{\perp}$, R) of initial conditions, giving the six independent RF diffusion coefficients in 3D constant-of-motion space. The method follows the formalism of Refs. [2,3]. For comparison, we have the zero-banana-width RF diffusion coefficients calculated in the AORSA code[1]. Comparison is more directly achieved in the present work by subtracting off the perpendicular guiding center drifts using a fictitious force in the Lorentz equation, $\mathbf{F}_{\perp} = \mathbf{u}_{\mathbf{gc}} \times \mathbf{B}$. This removes the finite banana width effects, but leaves correlation, finite gyro-radius, and other effects. The integration of (64 radii) × (128 $u_{\perp}$) × (256 $u_{\|}$) × (8 gyro-phase) × (8 toroidal angle) starting positions (134M Lorentz orbits) for a single toroidal mode is well-parallelized and takes 1 hour on 2048 cores, and 8 times as long summing over 101 complex toroidal modes; these global calculations are enabled by recent advances in supercomputing[4].

The DC code is similar to the MOKA code[5], but has been coupled to the CQL3D Fokker-Planck code[6] and AORSA to obtain a time-dependent, noise-free solution to the ICRF heating problem across the whole plasma width.

The final section gives results from the sMC Monte Carlo code, addressing finite-orbit-width effects in C-Mod, using AORSA QL diffusion coefficients.

2. Correlation Effects with the DC Code and Comparisons with AORSA QL Coefficients

In this report, focussed on an ITER relevant discharge in the Alcator C-Mod tokamak, we compare the ICRF diffusion coefficients calculated by DC, which includes correlations, with the AORSA QL coefficients derived using the random-phase approximation and neglecting all inter-resonance correlations. The toroidal variation of the RF fields is accounted for by Fourier decomposition into 101 modes with n_{ϕ} = [-50,+50], described in [7]. C-Mod is in an

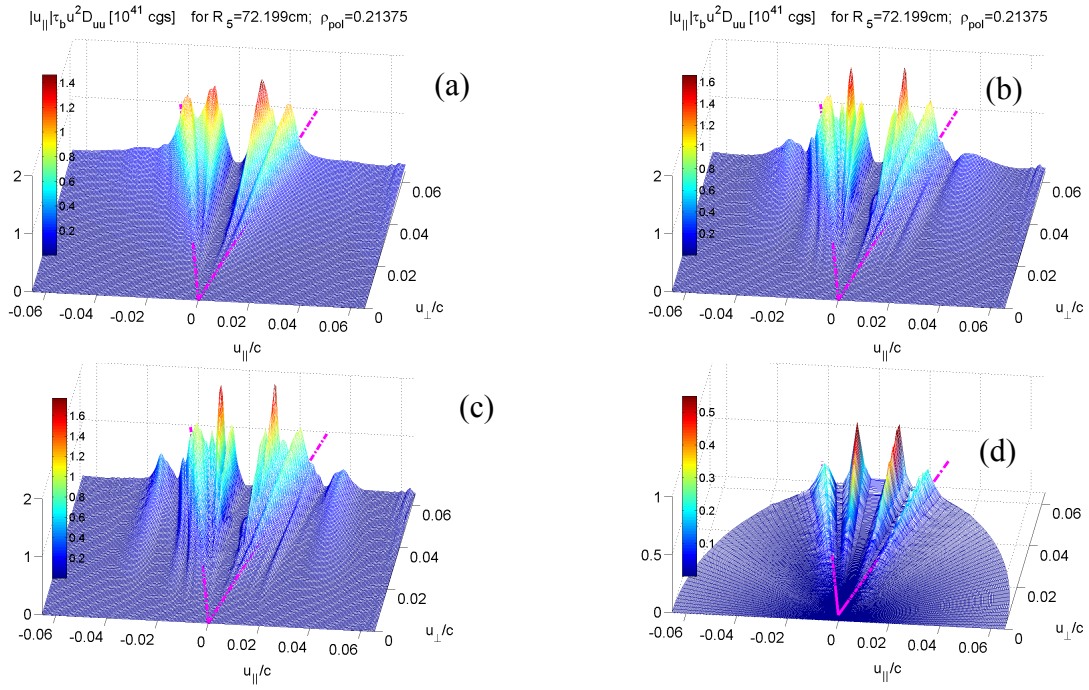

Fig. 1. D_{uu} diffusion coefficients: (a) From DC, 1 poloidal turn; (b) From DC, 2 turns; (c) From DC, 4 turns; and (d) From AORSA QL coefficient calculation. These coefficients, for C-Mod minority H, are at the same radii near the peak of the radial absorption profile, and give approximately equal power absorption.

intermediate toroidal damping regime with the waves propagating toroidally, being damped in ~0.5 toroidal turns. An ITER case gives single pass absorption with little toroidal propagation, whereas NSTX HHFW waves extend around the tokamak from the antenna with damping length of several toroidal turns[6]. Fig. 1(a-c) compares the velocity space D_{uu} diffusion coefficient calculated by DC for 1,2, and 4 complete turns in the poloidal plane. The fig 1(b) coefficient for 2 turn shows significantly greater pitch angle dependence than the single turn results in 1(a); fig. 1(c) for 4 turns shows little additional correlation effects. Peaks of the Fig. 1 coefficients are 1.46(1 turn), 1.66(2 turns), 1.77(4 turns), and 0.55(AORSA QL), in accord with heuristic expectations for correlations which are reaching maximum effect. All three DC coefficient radial sets show remarkable agreement in radial power absorption, shown in Fig. 2. The overall conclusion is that correlation effects in this case are fully developed after two poloidal turns. For ITER, only one turn may be necessary, given the toroidal precession of the particles and the very toroidally localized ICRF field[6]. Other cases such as NSTX may require additional poloidal turns to realize the full effects of resonance correlations. A further noteworthy feature on Fig. 1(b-c) and Fig. 2, is the remarkable accuracy obtained for the DC D_{uu} coefficient: the diffusion coefficients are essentially unchanged when calculated at the end of 2 or

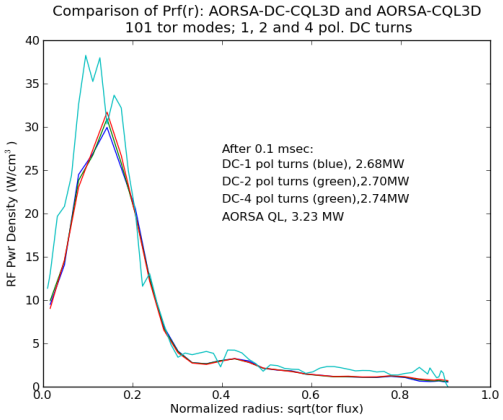

Fig. 2. Radial profile of ICRF power deposition derived from DC with 1,2, and 4 poloidal turns, and from AORSA QL coefficients.

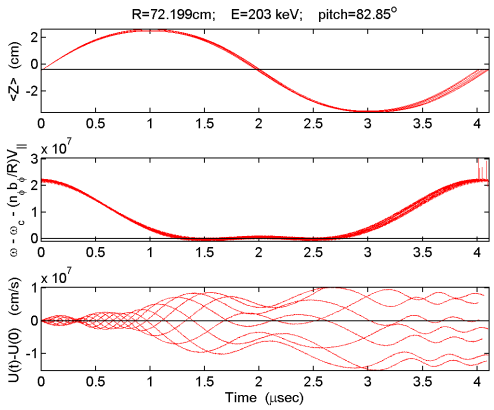

Figure 3. DC orbits originating on the equatorial plane at the same location as in Fig. 1, launched with pitch angle inside the trapped-passing boundary and such that the banana tips just pass through resonance. AORSA would show 4 separate diffusion contributions. The eight orbits are launched equispaced in gyrophase.

4 turns, and the power absorption profiles do not significantly evolve.

Fig. 2 results are obtained with the CQL3D Fokker-Planck code[7] for the canonical C-Mod, 4% minority H, *Te*=*Ti*=2.9 keV case[8], evolving the distributions for a short 0.1 msec time. The power density profiles and total power show good agreement, 20% difference in total power, between profiles calculated with "zero-banana-width" DC diffusion coefficients, and AORSA calculated Kennel-Engelmann[9] diffusion coefficients. The RF velocity-space "kicks" are completely correlated in DC, but are randomly phased for each resonance in AORSA. Moreover, there is no accounting for higher order tangent resonant effects. However, the rf diffusion coefficients are quite different, as shown in Figure 1(a) from DC and 1(d) from AORSA. The AORSA coefficients are wider in pitch angle, with peak value about one third the DC coefficients. Figure 3 shows details of the orbits from the DC calculation on a flux surface with radius 4 cm, and the cyclotron layer about 2 cm inboard of outer equatorial plane crossing. The resonance condition shown in the central panel is met four times. However, the DC orbit remains highly correlated over half the orbit, in contra- distinction to AORSA which gives four separate random-phase diffusion contributions in such a case. From a generalized "Stix-model", below, the effect of correlations is to redistribute the diffusion coefficient in pitch angle, enhancing it at some pitch angles but reducing at other, thus giving no change in flux surface average power absorption per volume for isotropic distributions. That is, $\langle p_{RF}\rangle = \int d^3u_0 |u_{\|0}\tau_b| E (\partial f_0/\partial t)_{RF}$ where $E = (1/2)mu^2$ is energy, and $(\partial f_0/\partial t)_{RF}$ is the quasilinear diffusion operator; after integration with isotropic distribution, only the term proportional to D_{uu} remains. Thus even though there is additional pitch angle structure in the DC-derived coefficients, for isotropic distributions as at early times in the ICRF turn on, the power absorption profiles remain close for DC and AORSA.

Figure 4 illustrates the reinforcement or cancellation of the velocity space kicks which occur due to correlation between two resonant interactions using a simplified model built on an ion cyclotron damping model in Stix's ICRF paper[10]. Plasma with circular flux surfaces is assumed, with toroidal magnetic field varying as R^{-1} and cyclotron resonance passing through the magnetic axis. Stix's equation for the cyclotron interaction is

$$\frac{du_\perp}{dt} + i\,\Omega(t)u_\perp = \frac{q}{m}E_+ \exp(-i\omega t), \quad \text{where } u_\perp \equiv u_x + iu_y \text{ is the complex perpendicular}$$

velocity, and $\Omega(t)$ is the local cyclotron frequency along the ion orbit. An approximate solution given by Stix for one pass through resonance is $u_\perp(t) = (u_\perp(-\infty) + U)\exp(-i\int \Omega dt)$

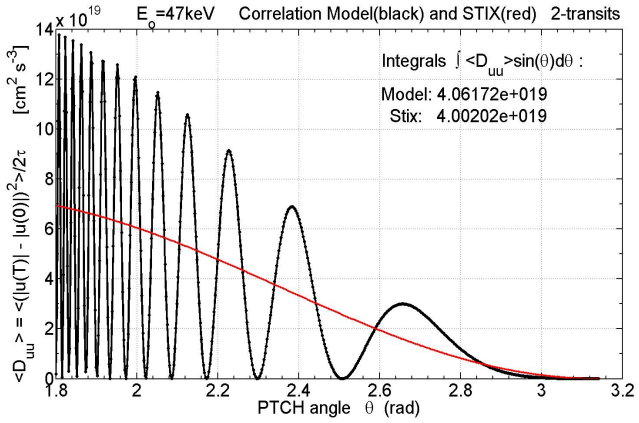

Fig. 4(a). Gyro-phase average diffusion coefficient after two transits of resonant surface. The E_+ field peaks near the resonance surface, which passes through the magnetic axis.

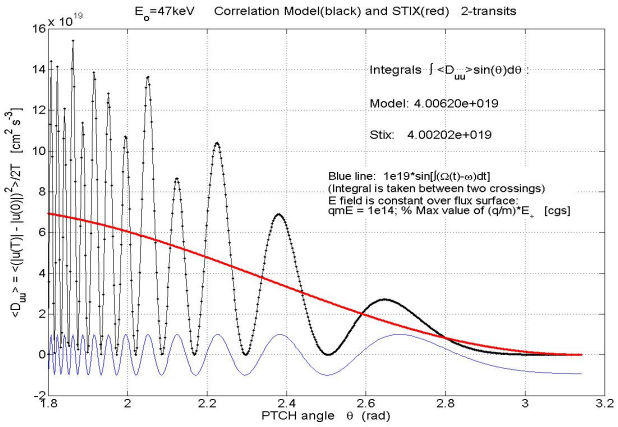

Fig 4(b). Same as Fig. 4(a), except that the E_+ field is constant across the poloidal cross-section, indicating little change in results due to starting particles in the non-resonant fields.

where $U \equiv \frac{q}{m} E_+ \left(\frac{2\pi i}{d\Omega/dt} \right)^{1/2}$. From this, we find an expression for the phase average diffusion coefficient for a single pass through the resonance region which agrees within small numerical error with what is obtained by numerical integration of the above differential equation for $u_\perp$. In Figure 4(a), we compare numerically determined phase average diffusion after two correlated passes of the resonance region, with the analytic expression for two uncorrelated passes as will be obtained with quasilinear theory. This shows that the correlations for two resonances double the maximum diffusion coefficient, relative to the uncorrelated interaction with two resonances. However, the sin(θ_0)-weighted integrals over pitch angle of the diffusion coefficient, proportional to rf power absorption on an isotropic distribution, are equal to within numerical error. The same general result is obtained with four successive resonances, as happens for trapped particles during one poloidal transit. Thus, this model appears to explain both the large variation of the DC diffusion coefficients relative to AORSA shown in Figure 1, and the excellent agreement between the power absorption in Figure 2 at small times in solution of the Fokker-Planck equation. The correlations shift the diffusion coefficient around in pitch angle, but for an isotropic ion distribution the power absorption is unaffected.

A concern in these calculations was the effect of starting the ion orbits within the rf fields, giving fictitious "diffusion" due to the non-resonant fields. Figure 4(b) with the simplified

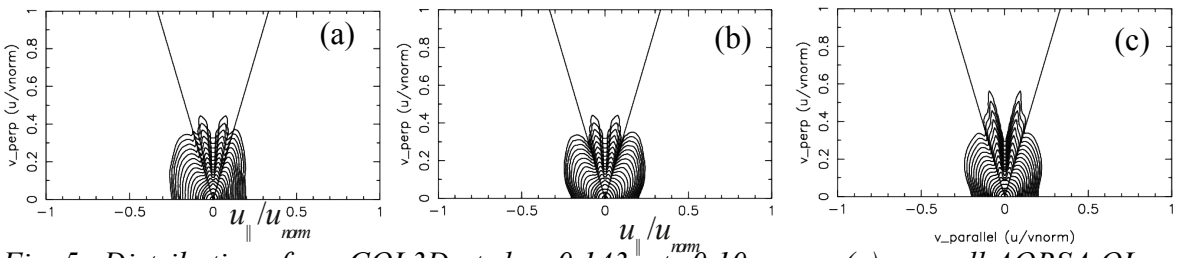

Fig. 5. Distributions from CQL3D at rho=0.143a, t=0.10 msec. (a) uses all AORSA QL diffusion coefficients; (b) uses only AORSA D_{uu}; and (c) uses only DC D_{uu}. Corresponding contour levels are within 2% of each other, and cover 12 orders of magnitude

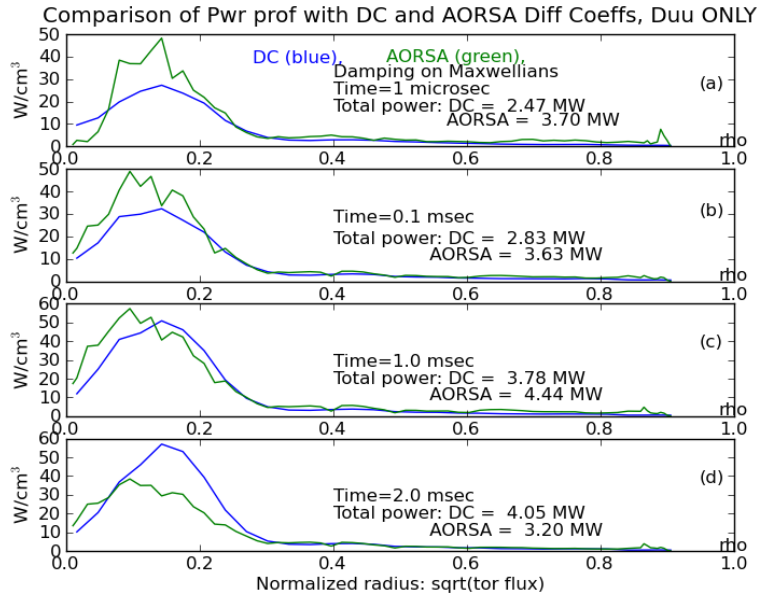

Fig. 6. Radial profiles of ICRF power absorption, from DC (blue) and AORSA (green). The time development of the distributions leads to cumulative differences in the profiles as a result of differences in the rf diffusion coefficient.

model but with the E_+ field uniform in the poloidal cross-section, indicates this is not a substantial affect, particularly when averaged over pitch angle. Although DC produces accurate D_{uu} coefficients, recent work has shown that coefficients involving the pitch angle are dominated by numerical error, and this is being addressed. The pitch angle related RF diffusion terms do not have a major effect, as seen in Fig. 5, and hence are omitted from the present calculations. Fig. 5 compares distributions near peak absorption with (a) all ICRF diffusion coefficients. And (b) with only D_{uu}; results are quite close to each other. Fig. 5(c) uses only the D_{uu} from DC, and displays the similar "rabbit ear" expansion due to orbits such as in Fig. 3.

With additional Fokker-Planck time steps, the pitch angle variation of distribution functions becomes different in the DC and AORSA diffusion coefficient cases at C-Mod ICRF power levels, and thus differences develop in the power absorption profiles. Enhanced distribution function tails at pitch angles of correlated RF "kicks" increase the absorption, as in Figure 6. At short times, 1 microsec, there is a issue for both DC and AORSA when damping primarily on relatively cold Maxwellians (central ion temperature is 2.9 keV) of inaccuracy of the power absorption calculated with diffusion coefficients on a grid up to 2 MeV. For times greater than ~2.0 msec in the present study, substantial power absorption extends up the upper velocity grid boundary, thus creating inaccuracy beyond this time as the ion tail population continues to grow. Power absorption at intermediate times is more reliable. Future work will include extending the velocity grid as needed. Also, finite orbit effects are becoming very important at 2 MeV in C-Mod, and will be an important loss mechanism of the tail, preventing the buildup of very energetic tail particles.

Past work with DC[11] has found close agreement between single (dominant) toroidal mode results and the 101 toroidal mode case focused upon in this report. For example, power absorption was 3.89 MW from DC and 3.80 MW from AORSA coefficients, at t=0.5 msec in the same simulation, with similar radial power profiles.

Our tentative conclusions from these comparisons between correlated DC and uncorrelated QL AORSA ICRF coefficients are that the broad toroidal spectrum resulting from sufficient damping in cases in C-Mod, and particularly in ITER, leads to "saturation" of correlation effects after one or two poloidal turns of the ions. If the toroidal damping length exceeds the

machine circumference, then more poloidal turns are required. But even in single toroidal mode simulations with just one poloidal turn to obtain DC rf coefficients, simply neglecting further correlations which are particularly important for a single toroidal mode, still leads to reasonably accurate C-Mod simulation. It appears that uncorrelated QL theory provides sufficient accuracy for practical simulations in the present C-Mod case. Future work will focus on increases in speed and accuracy of the DC calculation, further quantification of the nature of deviations from QL theory, investigation of high rf power effects on diffusion, and multiple-resonances per gyro-period as occur for energetic ions in the NSTX high harmonic fast wave experiments.

3. SMC Monte Carlo Investigation of Finite-Orbit-Width Fast Ions in C-Mod

Based on the above conclusions, investigating the impact of including finite ion orbit-widths using the QL diffusion coefficients derived from a single toroidal mode solution of the full-wave AORSA code is justified. As with the AORSA-DC-CQL3D coupling, here we again utilise an iterative coupling between an update to the ion distribution function, under the influence of RF heating and Coulomb collisions, and the AORSA full-wave code. However, instead of the finite difference CQL3D Fokker-Planck code, we use the simple Monte-Carlo (sMC) code [12]. sMC integrates 5D guiding center particle orbits in the presence of pitch angle and energy scattering on a single Maxwellian background species. The collision operators used are those presented in [13]. Only Coulomb collisions with a thermal background and the RF source are included in the model (hence the "simple" in sMC), and the integration of particle orbits is done in cylindrical coordinates (both space and velocity) with a Runge-Kutta 4 algorithm. The reasons for utilizing a Monte-Carlo (MC) particle approach for the QL update of the ion distribution in a study of finite ion orbit effects are as follows: (i) Finite ion orbit drift from magnetic flux surfaces are naturally included, and are easily removed for comparison. (ii) The requirement that the energy kick given to a particle crossing a resonance be some small fraction of it's total energy, i.e., diffusive, is a requirement only to the Fokker-Planck approach of CQL3D and not to a MC particle code solving a Langevin equation. This could be important for the minority heating problem where an energetic tail is drawn out of a thermal background. (iii) RF induced radial diffusion is naturally included.

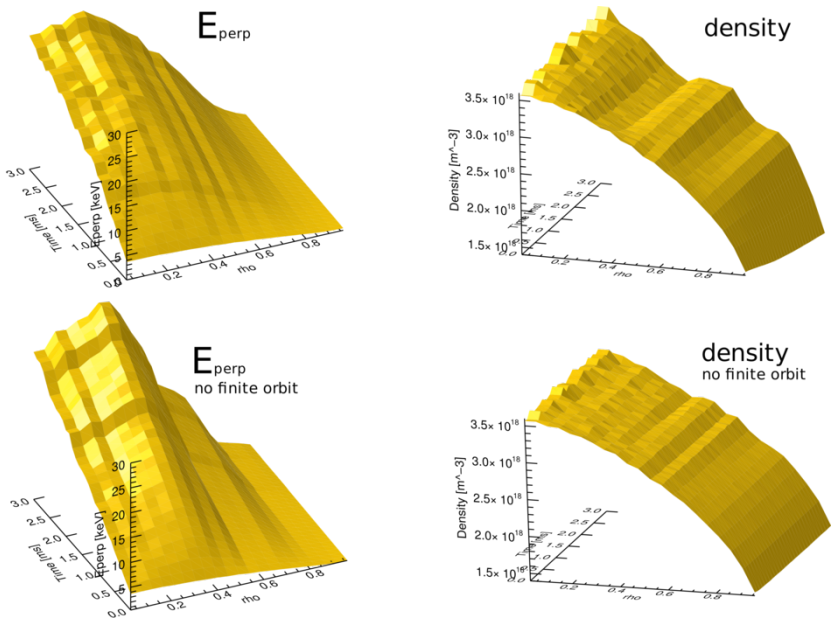

Fig. 7. Time evolution of the flux surface averaged perpendicular energy per particle and density for 3% minority H heating scenario in C-Mod.

Also, in contrast to many other [e.g., 13,14] MC ion cyclotron heating codes, instead of applying the usual Stix QL "kick" expression [15, 13] as particles cross resonances, sMC utilizes the AORSA QL diffusion coefficients described above. sMC is then able to include the complete wavenumber spectrum and up-shift in $k_{||}$ due to the poloidal field whereas the "kick" approach requires a single parallel wavenumber (usually approximated as $k_{||} = n_\phi/R$), and the perpendicular wavenumber $k_\perp$ to be estimated from the cold plasma dispersion relation. Therefore, the AORSA- sMC iteration is applicable to scenarios such as beam heating on DIII-D and NSTX. Furthermore, sMC utilizes leadership class computing facilities (e.g., Cray XT5 supercomputers at NERSC and NCCS) and as such is able to track particles below the thermal velocity where the collision frequency becomes large allowing the study of minority heating scenarios.

The impact of finite ion orbits is studied by performing iterative AORSA-sMC calculations with and without finite ion orbits. Finite ion orbits can result in a broader collisional power transfer profile, additional resonant surface crossings, RF induced spatial transport and prompt losses to the vessel wall. However, these effects are important only when the ion energies are sufficient such that their orbits deviate from magnetic flux surfaces. Such scenarios include energetic ion tail formation, beam heating and fusion alphas. Here we focus on tail formation for minority heating on C- Mod. Figures 7 and 8 show the time development of stored perpendicular energy and a 3% minority H distribution function $f_H(u_\perp, u_{||})$, respectively, for a single toroidal mode (n_ϕ=10), minority heating scenario with 2.4MW of RF power at 80MHz in a D bulk plasma with core temperature of 3.6keV. Plasma profiles are parabolic flux functions as indicated by the reduction in temperature with increasing flux (rho) seen in Fig. 7, and in the top row of Fig. 8. The impact of including finite ion orbits can be seen by comparing the top and bottom rows of Fig. 7. The top left panel clearly shows a broader power deposition profile than for the no-finite-orbit case (lower left panel). Also,

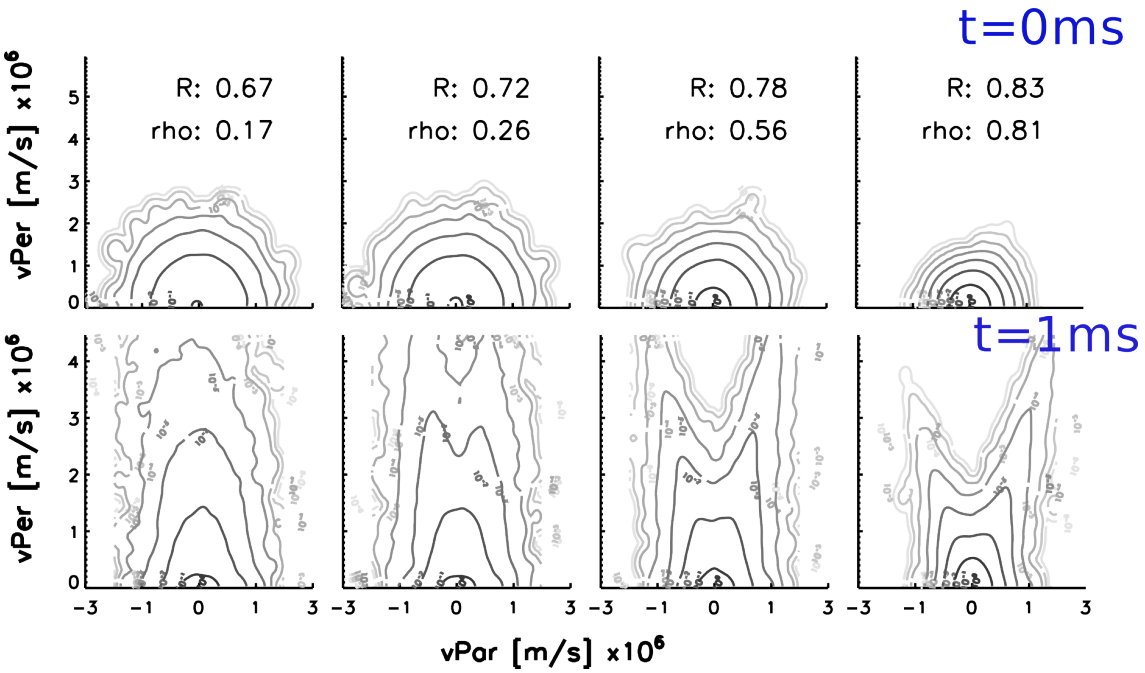

Fig. 8: H distribution $f_H(u_\perp, u_{||})$ at z = 0 for the initial Maxwellian and 1ms iteration.

significant RF induced radial transport is seen in the time development of the density profile for the case where finite ion orbits are included (top right) compared to (lower right). The ion density profile has developed structure away from the magnetic axis, as well as showing prompt losses to the wall.

The primary goal of this work was to test the direct use of the AORSA diffusion tensor in a MC particle code. The implementation in sMC was successfully verified against CQL3D for cases where finite ion orbit effects are not significant. Future work will involve using sMC to compare the validity of the standard "kick" type MC operator approximations in scenarios such as High Harmonic Fast Wave heating on NSTX where up-shift plays an important roll. Additionally, the implementation used to apply the AORSA diffusion coefficients in sMC will ultimately be installed in the more comprehensive TRANSP framework [16], specifically in NUBEAM, [17] where additional physics, other than the collision and RF operators used here, are included.

Research supported by USDOE Contracts DE-FC02-01ER54649, DE-FC02-01ER54648, DE-FG02-04ER54744, and DE-AC05-00R22725 with UT-Battelle, LLC.

REFERENCES

1. E.F. Jaeger, L.A. Berry, et al., Nucl. Fusion 46, (2006) S397-S408.
2. A. Kaufman, Phys. Fluids 15, 1063 (1972).
3. L-G. Eriksson and P. Helander, Phys. Plasmas 1, 308 (1994).
4. This research used resources of the National Energy Research Scientific Computing Center, supported by the Office of Science of the U.S. Dept. of Energy, Contract DE-AC02-05CH11231.
5. V. Bergeaud, F. Nguyen, A. Becoulet and L-G. Eriksson, Phys. of Plasmas 8, 139 (2001).
6. R.W. Harvey and M.G. McCoy, "The CQL3D Fokker-Planck Code", IAEA TCM, on Advances in Simulation and Modeling of Thermonuclear Plasmas, Montreal (1992).
7. E.F. Jaeger, L.A. Berry, et al., Phys. of Plasmas 15, 072513 (2008).
8. A. Bader, P. Bonoli, et al., Bull. Amer. Phys. Soc., (AIP, NY, 2008), Paper PP6.00100.
9. C. Kennel and F. Engelmann, Phys. Fluids 9 , 2377 (1966).
10. T.H. Stix, Nucl. Fus. 15, 737 (1975).
11. R.W. Harvey, Yu. Petrov, E.F. Jaeger, L.A. Berry et al., Proc. of Euro. Phys. Soc. Mtg., P1.090, Sofia, Bulgaria (2009)..
12. Green, D. L., et al., J. Phys.: Conf. Series, 180, 012058 (2009), doi:10.1088/1742-6596/180/1/012058
13. [13] Kovanen, M. A., et al., Nucl. Fusion, 32, 5, 787-799 (1992)
14. Choi, M. et al., Nucl. Fusion, 46, S409-S415, (2006), doi:10.1088/0029-5515/46/7/S03
15. T. H. Stix, Nucl. Fusion 15, 737-754 (1975)
16. D. McCune, et al., American Physical Society, 48th Annual Meeting of the Division of Plasma Physics, (2006), #JP1.121.
17. A. Pankin, et al., Computer Phys. Comm., 159, 3, 157-184, (2004), doi:10.1016/j.cpc.2003.11.002